THE JOURNAL OF PHYSICAL CHEMISTRY Letters

pubs.acs.org/JPCL Letter

Supported Molybdenum Carbide Nanoparticles as Hot Hydrogen Reservoirs for Catalytic Applications

Marc Figueras, Ramón A. Gutiérrez, Francesc Viñes,* Pedro J. Ramírez, José A. Rodriguez,* and Francesc Illas

Cite This: *J. Phys. Chem. Lett.* 2020, 11, 8437−8441 Read Online

ACCESS | Metrics & More | Article Recommendations | Supporting Information

ABSTRACT: Transition metal carbides have been long proposed as replacements for expensive Pt-group transition metals as heterogeneous catalysts for hydrogenation reactions, featuring similar or superior activities and selectivities. Combining experimental observations and theoretical calculations, we show that the hydrogenating capabilities of molybdenum carbide can be further improved by nanostructuring, as seen on MoC_y nanoclusters anchored on an inert Au(111) support, revealing a more prominent role of Mo active sites in the easier H_2 adsorption, dissociation, H adatom diffusion, and elongated chemisorbed H_2 Kubas moieties formation when compared to the bulk δ-MoC(001) surface, thus explaining the observed stronger H_2 interaction and the larger formation of CH_x species, making these systems ideal to catalyze hydrogenation reactions.

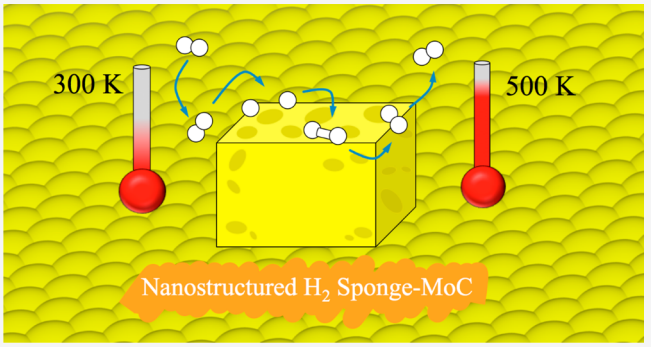

Hydrogenation reactions are common in many industrial processes, e.g., in the petrochemical plastic generation,[1] the saturation of vegetable oils polyunsaturated fat acids in food chemistry,[2] or in environmental chemistry, converting greenhouse carbon dioxide (CO_2) into greener chemicals.[3] Hitherto, hydrogenations have been mostly catalyzed using scarce and expensive Pt-group metals.[1,4] During the last decades, transition Metal Carbides (TMCs) have emerged as an alternative, often displaying superior activities and selectivities for a wide variety of relevant hydrogenation reactions.[3−9]

Consequently, considerable research efforts have been undertaken aimed at tailoring the TMCs hydrogenating capabilities. To this end, TMC nanoparticles (NPs) have been often used, deposited on oxide or zeolite-type supports.[10−12] Studies on the H_2 adsorption on TMCs extended single-crystal surfaces have shown complex phenomena related to H_2 adsorption and dissociation,[7,8] the diversity of easily interconvertible surface hydrogen species,[13] and the importance of H-coverage in lowering reaction energy barriers.[14] Unfortunately, it is yet not clear how to extrapolate this behavior to the supported TMC NPs, seriously hampering the rational design of novel hydrogenation catalysts.

We recently started a research program to investigate the intrinsic reactivity of free and Au-supported TMC nanoparticles.[15] Inspired by the tuning capabilities of the inverse oxide/metal catalysts,[16] MoC_y clusters were stabilized over an inert support, Au(111).[17] This produced systems able to dehydrogenate cyclohexene[18] and dissociate methane at room temperature.[15] The enhanced chemical activity is consistent with the CO_2 hydrogenation trends seen on carbon-supported TMC NPs.[19] Here, nanostructuring is exploited to tune the TMCs NPs reactivity on the basis of size, shape, and composition control. Combining X-ray Photoelectron Spectroscopy (XPS), Temperature-Programmed Desorption (TPD), and Density Functional Theory (DFT) based calculations, we show that $MoC_{1.1}$ nanostructures supported on Au(111) can act as hot H_2 reservoirs. We provide evidence that this behavior results from the combination of thermodynamic stability, diversity of H_x* species, easy H_2* dissociation and H* adatoms diffusion, an active role of low-coordinated Mo sites, and the promotion of Kubas complexes, all being the cornerstone of using MoC_y as ideal candidates for tailored hydrogenation catalytic reactions.

We start by examining the H_2 adsorption on a polycrystalline MoC surface reference. Previous studies showed a C/Mo ratio of 0.98 in this system,[20] very close to the 1.0 value for rocksalt δ-MoC. Figure 1 displays the C 1s XPS spectra collected before and after exposing bulk MoC to 1 Torr of H_2 at 300 K for 5 min. The initial C 1s peak at ∼282.4 eV corresponds to C

Received: August 26, 2020
Accepted: September 14, 2020
Published: September 22, 2020

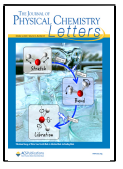

https://dx.doi.org/10.1021/acs.jpclett.0c02608
J. Phys. Chem. Lett. 2020, 11, 8437−8441

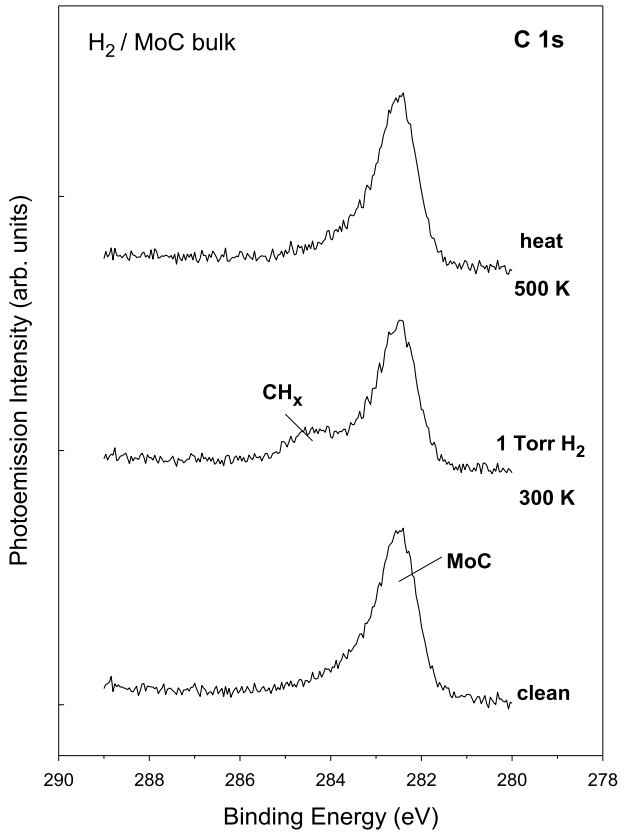

Figure 1. C 1s XPS spectra collected after dosing 1 Torr of H_2 to bulk MoC at 300 K with subsequent heating to 500 K. For comparison, the corresponding spectrum of the clean MoC is provided. The data were collected at an angle of 70° with respect to the surface normal to maximize surface contributions.

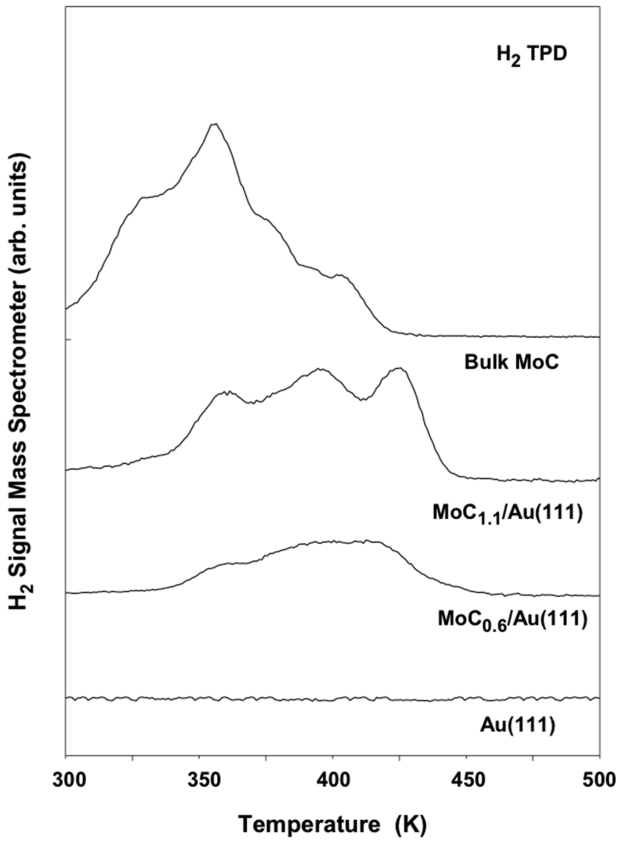

Figure 2. H_2 thermal desorption spectra collected after adsorbing hydrogen on bulk MoC, clean Au(111), and a gold substrate covered with 0.3 ML of $MoC_{1.1}$ or $MoC_{0.6}$. All the surfaces were exposed to 1 Torr of H_2 at 300 K for 5 min. The heating rate in the thermal desorption spectra is 2 K/s.

atoms in the δ-MoC surface.[15] There, H_2 adsorption and dissociation lead to a new feature at 284.0−284.5 eV assigned to the formation of CH_x groups on the MoC.[15,17,18] From the XPS peaks intensity, we estimate that the CH_x groups coverage is 0.2−0.3 monolayers (ML), which were removed by heating to 500 K for 1 min. Indeed, the TPD data in Figure 2 reveal that the hydrogen fully desorbs by 425 K, in a complex TPD spectrum where one can see clear peaks at 325, 350, and 400 K plus weak features at 370 and 380 K. This probably reflects the polycrystalline character of the MoC surface, which contains a large number of defective sites. By comparing to the TPD spectra of hydrogen on Pt(111),[21,22] one can estimate a hydrogen coverage of 0.93 ML, much larger than the 0.2−0.3 ML CH_x groups coverage seen in the XPS spectrum of Figure 1. Therefore, only a part of the surface hydrogen on the bulk MoC surface forms CH_x species, whereas a considerable amount involves H* adatoms on other active sites.

Au(111) surfaces were prepared containing 0.3 ML of either $MoC_{0.6}$ or $MoC_{1.1}$ nanoparticles following an earlier reported procedure.[15,17] This procedure leads to oxygen-free MoC nanoparticles where the C/Mo ratio varies from 0.6 to 1.1.[15,17] Scanning Tunnelling Microscopy (STM) images showed that these NPs are small (0.8−1.5 nm) and aggregate in the face-centered cubic (fcc) troughs located on either side of the elbows of the reconstructed Au(111) surface.[17] We found that the C/Mo ratio has a strong influence on the MoC_y NPs reactivity toward H_2, as seen in Figures 2 and 3, but in general the nanostructures displayed a behavior different from that of bulk MoC. In the case of $MoC_{0.6}$/Au(111), Figure 3A, a very small amount (0.05 ML) of CH_x was formed. This means that only a reduced fraction (∼30%) of the C atoms present on the surface (0.18 ML) are involved in formation of CH_x species, probably due to the strong bonds between C and Mo atoms in the NPs required to maintain the cluster integrity. From the TPD in Figure 2, we estimate that the total coverage of hydrogen adsorbed on the $MoC_{0.6}$/Au(111) surface is only 0.27 ML, substantially smaller than that seen on bulk MoC but consistent with the fact that we only had 0.3 ML of $MoC_{0.6}$ on the gold substrate.

A distinct behavior is seen for the dissociative adsorption of H_2 on $MoC_{1.1}$/Au(111), where a larger C/Mo ratio of 1.1 did not lead to a reactivity decrease. On the contrary, C atoms in $MoC_{1.1}$ NPs were significantly more reactive than in either the $MoC_{0.6}$ NPs or in bulk δ-MoC. Figure 3B shows strong C 1s XPS features at a binding energy of ∼284.6 eV, implying ca. 50% of the surface C atoms transformed into CH_x species. This process is fully reversible, as, upon heating to 500 K, H_2 desorbed without evolution of CH_4 or other light hydrocarbons. The reversible H_2 adsorption/desorption process was repeated several times (see Figure 3B and Figure S1 of the Supporting Information), and the C/Mo ratio was maintained in $MoC_{1.1}$/Au(111). The corresponding TPD spectrum in Figure 2 shows H_2 evolution at 360, 390, and 430 K, from which a total hydrogen coverage of 0.58 ML was estimated. This points to a H/C ratio close to 2, a value much larger than the one observed on bulk δ-MoC surfaces, posing $MoC_{1.1}$ NPs

https://dx.doi.org/10.1021/acs.jpclett.0c02608
J. Phys. Chem. Lett. 2020, 11, 8437−8441

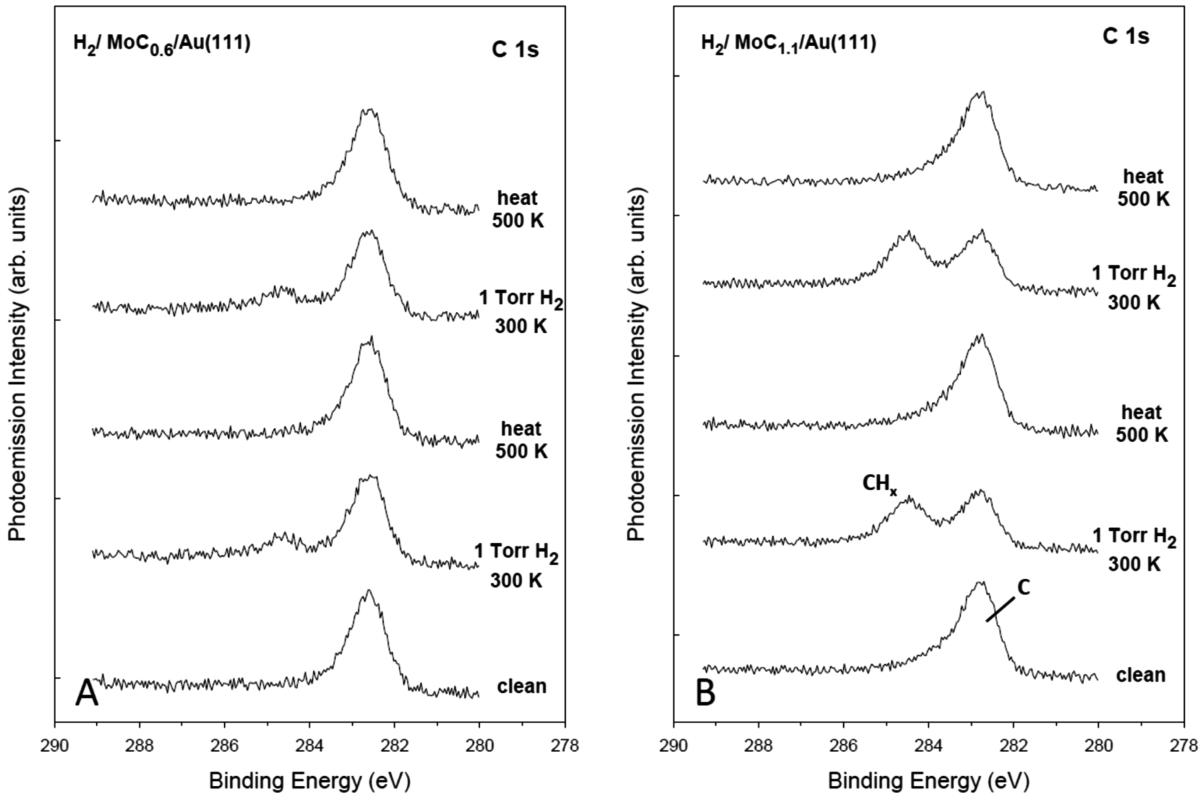

Figure 3. (A) C 1s XPS spectra collected after dosing 1 Torr of H_2 to $MoC_{0.6}$/Au(111) and (B) $MoC_{1.1}$/Au(111) at 300 K with subsequent heating to 500 K. The gold substrate was covered with 0.3 ML of $MoC_{0.6}$ or $MoC_{1.1}$ nanoparticles. The data were collected at an angle of 70° with respect to the surface normal to maximize surface contributions.

as hydrogen sponges, where H_2 can be easily adsorbed or desorbed, being hot hydrogen reservoirs for catalytic applications. The results for several cycles of hydrogen adsorption/desorption in Figure S1 indicate that the coverage for CH_x species on $MoC_{1.1}$/Au(111) was always close to 0.14 ML while being only near 0.04 ML on $MoC_{0.6}$/Au(111). This also points to $MoC_{1.1}$/Au(111) as an effective system for hydrogenation process.

To explain the remarkable results for $MoC_{1.1}$/Au(111), we carried out a DFT study using a stoichiometric $Mo_{12}C_{12}$ nanoparticle model supported on Au(111). Calculations were pushed toward a chemical accuracy below 0.04 eV using a Au(111) four-layered $p(6 \times 6)$ slab model with a 30 Å vacuum and using the Perdew–Burke–Ernzerhof (PBE)[23] exchange–correlation functional and including the D3 method proposed by Grimme to account for dispersion.[24] Further computational details are reported in the Supporting Information.

On the supported $Mo_{12}C_{12}$ NP, molecular H_2 and H adatoms attach with similar strength (see Figure 4), with H_2 preferring low-coordinated Mo sites, with an adsorption energy, E_{ads}, of up to −0.48 eV. Compared to a previous study for δ-MoC(001), which featured a stronger H_2 E_{ads} of −0.60 eV on-top of C atoms,[13] this involves here an active site switching from C to Mo. Aside, both δ-MoC(001) and $Mo_{12}C_{12}$/Au(111) prefer the H_2 dissociated state. Hence, the focus is on the stability of H*, which exhibits a preference toward corner C atoms, with an E_{ads} of −0.60 eV with respect to 1/2·H_2 and $Mo_{12}C_{12}$/Au(111), slightly stronger than on surface C atoms of δ-MoC(001), with an E_{ads} of −0.55 eV.[13] By assuming an order two desorption kinetics for H* — implying H* + H* recombination to H_2* prior to its desorption— and an estimate of desorption temperatures for the highest temperature peaks in Figure 1 via Redhead equation with pre-exponential values ranging 10^8–10^{13} s^{-1}, reveals a TPD shift toward higher temperatures of 28–19 K in $Mo_{12}C_{12}$/Au(111) relative to δ-MoC(001), in perfect agreement with the shift of ∼30 K as observed in Figure 2. Notice that the second peak of $MoC_{1.1}$/Au(111) could be assigned to H* on corner Mo atoms, with an E_{ads} of −0.54 eV, quite close, both in strength and in TPD peak position, to the low-coverage regular C sites on δ-MoC (001).[13] Finally, the peak at ∼355 K could be assigned to high-coverage H adatoms on regular (001) facet C atoms, sites in common for MoC_y NPs and δ-MoC (001) extended surfaces.

The distinct role of low-coordinated Mo sites on MoC_y for H adsorption relates to its E_{ads} of −0.54 eV, clearly stronger compared to the unfavorable interaction at Mo sites on δ-MoC(001),[13] which contributes to the to the aforementioned H_2 sponginess of supported MoC_y and the stronger interaction toward H adatoms upon or in the vicinity of low-coordinated Mo sites. It seems that the activity-killing ligand effect that C atoms have on neighboring Mo atoms, as featured on δ-MoC(001), gets counteracted by the lower Mo coordination, although particular electronic arrangements due to the nanoscale may play a role as well. Besides, on most stable H_2-anchoring Mo sites of $Mo_{12}C_{12}$/Au(111), H_2 features dissociation energy barriers as low as 0.2 eV (see Figure 4), thus halved compared to the extended δ-MoC(001) value of 0.39 eV.[13] Therefore, H_2 adsorption and dissociation is significantly promoted on supported MoC_y ($y > 1$) clusters, leading to a diversity of occupied C and Mo sites.

https://dx.doi.org/10.1021/acs.jpclett.0c02608
J. Phys. Chem. Lett. 2020, 11, 8437–8441

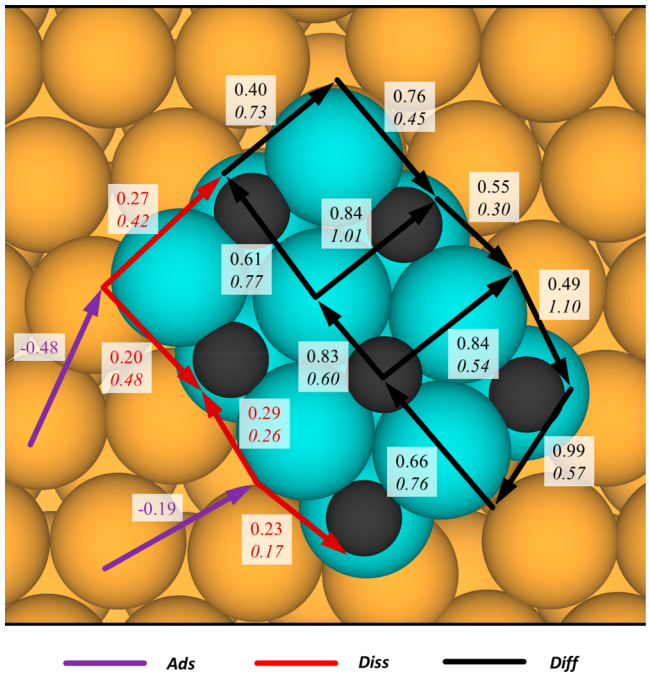

Figure 4. Top view of $Mo_{12}C_{12}$ supported on Au(111) surface. Black, blue, and orange spheres denote C, Mo, and Au atoms, respectively. H_2 adsorption sites are shown in purple, accompanied by adsorption energies, E_{ads}. Adsorbed H_2 dissociation energies are shown by red arrows, implying that one H adatom remains on-site, while the other moves to occupy a nearby site. H adatom diffusions are shown by black arrows, signaling initial to final locations. For H_2 dissociation and H diffusion, forward and backward energy barriers, E_b, are given in normal or italics fonts, respectively. All energy values are given in eV.

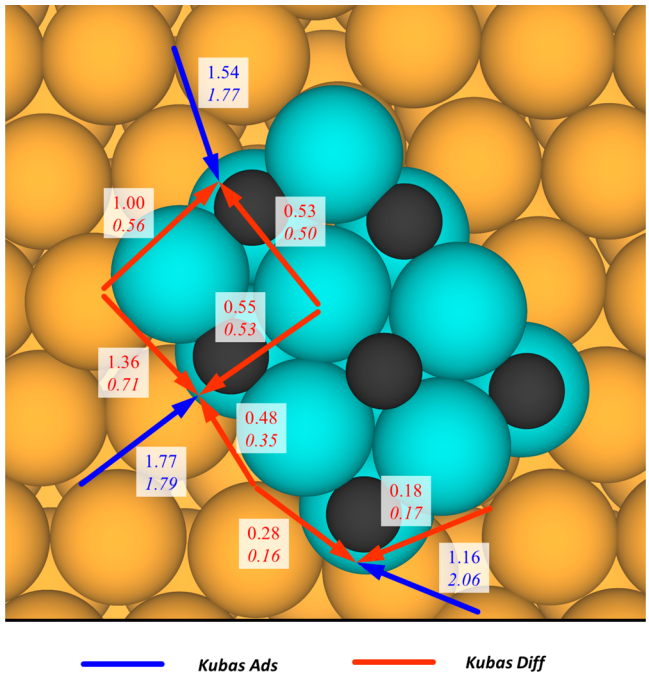

Figure 5. Top view of $Mo_{12}C_{12}$ supported on Au(111) surface. Kubas formation energy on low-coordinated C atoms are shown from gas-phase H_2 (blue) or through H adatoms recombination (red). In the latter a H adatom on a Mo site diffuses and interacts with the H-attaching surface C atom. Forward and backward energy barriers, E_b, are given in normal or italics fonts, respectively. All energy values are given in eV. Sphere color code as in Figure 4.

The mere H_2 dissociation on $Mo_{12}C_{12}$/Au(111) on the available aforementioned highly reactive sites would lead to a partial occupation of the MoC_y perimeter. Hence, a detailed analysis of the single H* diffusion has been performed, exemplified over the (001)-like facet; see Figure 4. The supported $Mo_{12}C_{12}$ nanoparticle features a rather complex network of H* diffusion steps, analyzed by having a look to the minimum barrier needed to be surmounted, so all sites could be occupied by H. For $Mo_{12}C_{12}$, this E_b is 0.76 eV, smaller than the equivalent value of 0.95 eV on δ-MoC(001),[13] implying that H* diffusion is also well promoted on nanostructured MoC_y model catalysts.

Finally, to explain the preferential CH_x formation on MoC_y nanoclusters with $y \sim 1$, the possibility of having a Kubas CH_2 structures has also been considered.[13] The direct Kubas formation on low-coordinated C atoms of $Mo_{12}C_{12}$ can be rapidly dismissed due to the large energy barriers involved, ranging 1.2−1.8 eV; see Figure 5. However, Kubas structures can be formed from diffusing H* adatoms on the MoC_y cluster. On each site, Kubas formation reaction paths exist with rather low energy barriers, from 0.18 to 0.55 eV, especially when compared to the equivalent barriers on δ-MoC(001) ranging 1.07−1.92 eV.[13] Thus, Kubas CH_2 structures can be easily formed on MoC_y NPs by H* diffusion processes, freeing neighboring Mo sites to further adsorb and dissociate H_2, a key aspect for the H_2 sponginess of MoC_y ($y \sim 1$) NPs and its high H_2 storage/release potential. Note that the present results permit us to understand the difference in H capacity of the two types of particles; since H prefers bonding to C atoms, either directly or as Kubas complexes, it appears that $MoC_{0.6}$ NPs, having fewer C atoms, have fewer active sites for H. Moreover, in such NPs, the carbons are more tightly bound to Mo, i.e., more saturated, and so less chemically active toward the CH_x formation.

All in all, on the basis of the above results, one can firmly state that, compared to δ-MoC(001), MoC_y ($y \sim 1$) NPs supported on Au(111) feature a stronger H_x affinity and a larger site diversity, with significantly reduced H_2 dissociation, H adatom diffusion, and CH_2 Kubas species formation energy barriers. These are key points in explaining the observed reversible H_2 sponginess on these systems Such inverse carbide/support catalysts are thus envisaged as promising hydrogenating catalysts, e.g., for ethylene hydrogenation, where both a high H coverage and easy H diffusion were found to be key for an easier and improved effective catalytic performance compared to late, Pt-group TMs.[14]

■ ASSOCIATED CONTENT

Supporting Information

The Supporting Information is available free of charge at https://pubs.acs.org/doi/10.1021/acs.jpclett.0c02608.

Experimental and computational details and a figure of the amounts of CH_x species generated on the MoC_y/Au(111) systems (PDF)

■ AUTHOR INFORMATION

Corresponding Authors

Francesc Viñes − *Departament de Ciència de Materials i Química Física & Institut de Química Teòrica i Computacional (IQTCUB), Universitat de Barcelona, 08028 Barcelona,*

https://dx.doi.org/10.1021/acs.jpclett.0c02608
J. Phys. Chem. Lett. 2020, 11, 8437−8441

Spain; orcid.org/0000-0001-9987-8654; Email: francesc.vines@ub.edu

José A. Rodriguez − *Chemistry Department, Brookhaven National Laboratory, Upton, New York 11973, United States*; orcid.org/0000-0002-5680-4214; Email: rodriguez@bnl.gov

Authors

Marc Figueras − *Departament de Ciència de Materials i Química Física & Institut de Química Teòrica i Computacional (IQTCUB), Universitat de Barcelona, 08028 Barcelona, Spain*

Ramón A. Gutiérrez − *Chemistry Department, Brookhaven National Laboratory, Upton, New York 11973, United States; Facultad de Ciencias, Universidad Central de Venezuela, Caracas 1020-A, Venezuela*

Pedro J. Ramírez − *Facultad de Ciencias, Universidad Central de Venezuela, Caracas 1020-A, Venezuela; Zoneca-CENEX, R&D Laboratories, Alta Vista, 64770 Monterrey, Mexico*

Francesc Illas − *Departament de Ciència de Materials i Química Física & Institut de Química Teòrica i Computacional (IQTCUB), Universitat de Barcelona, 08028 Barcelona, Spain*; orcid.org/0000-0003-2104-6123

Complete contact information is available at: https://pubs.acs.org/10.1021/acs.jpclett.0c02608

Notes

The authors declare no competing financial interest.

The data that support the findings of this study are available from the corresponding authors upon reasonable request.

■ ACKNOWLEDGMENTS

The research carried out at the Universitat de Barcelona has been supported by the Spanish MICIUN/FEDER RTI2018-095460−B-I00 and María de Maeztu MDM-2017-0767 grants and, in part, by Generalitat de Catalunya 2017SGR13 and XRQTC grants. This manuscript has been authored by employees of Brookhaven Science Associates, LLC under Contract No. DE-SC0012704 with the U.S. Department of Energy. F.I. acknowledges additional support from the 2015 ICREA Academia Award for Excellence in University Research. Computational resources provided by the Red Española de Supercomputación (RES) grants QS-2020-1-0007 and QS-2019-3-0004 are fully acknowledged.

■ REFERENCES

(1) Ebrahimi, M.; Simonovis, J. P.; Zaera, F. Near-Unity Reaction Probability in Olefin Hydrogenation Promoted by Heterogeneous Metal Catalysts. *J. Phys. Chem. Lett.* **2014**, *5*, 2121−2125.

(2) Emken, E. A.; Frankel, E. N.; Butterfield, R. O. Homogeneous Catalytic Hydrogenation of Unsaturated Fats: Metal Acetylacetonates. *J. Am. Oil Chem. Soc.* **1966**, *43*, 14−18.

(3) Posada-Pérez, S.; Ramírez, P. J.; Gutiérrez, R. A.; Stacchiola, D. J.; Viñes, F.; Liu, P.; Illas, F.; Rodriguez, J. A. The Conversion of CO_2 to Methanol on Orthorhombic β-Mo_2C and Cu/β-Mo_2C Catalysts: Mechanism for Admetal Induced Change in the Selectivity and Activity. *Catal. Sci. Technol.* **2016**, *6*, 6766−6777.

(4) Zhang, L.; Zhou, M.; Wang, A.; Zhang, T. Selective Hydrogenation over Supported Metal Catalysts: From Nanoparticles to Single Atoms. *Chem. Rev.* **2020**, *120*, 683−733.

(5) Levy, R. B.; Boudart, M. Platinum-Like Behavior of Tungsten Carbide in Surface Catalysis. *Science* **1973**, *181*, 547−549.

(6) Hwu, H. H.; Chen, J. G. Surface Chemistry of Transition Metal Carbides. *Chem. Rev.* **2005**, *105*, 185−212.

(7) Koverga, A. A.; Flórez, E.; Dorkis, L.; Rodriguez, J. A. CO, CO_2, and H_2 Interactions with (0001) and (001) Tungsten Carbide Surfaces: Importance of Carbon and Metal Sites. *J. Phys. Chem. C* **2019**, *123*, 8871−8883.

(8) Silveri, F.; Quesne, M. G.; Roldán, A.; de Leeuw, N. H.; Catlow, C. R. A. Hydrogen Adsorption on Transition Metal Carbides: a DFT Study. *Phys. Chem. Chem. Phys.* **2019**, *21*, 5335−5343.

(9) Schaidle, J. A.; Thompson, J. A. Fischer−Tropsch Synthesis over Early Transition Metal Carbides and Nitrides: CO Activation and Chain Growth. *J. Catal.* **2015**, *329*, 325−334.

(10) Shou, H.; Davis, R. J. Multi-Product Steady-State Isotopic Transient Kinetic Analysis of CO Hydrogenation over Supported Molybdenum Carbide. *J. Catal.* **2013**, *306*, 91−99.

(11) Vo, D.-V. N.; Adesina, A. A. Fischer−Tropsch Synthesis over Alumina-Supported Molybdenum Carbide Catalyst. *Appl. Catal., A* **2011**, *399*, 221−232.

(12) Gao, J.; Zheng, Y.; Fitzgerald, G. B.; de Joannis, J.; Tang, Y.; Wachs, I. E.; Podkolzin, S. G. Structure of Mo_2C_x and Mo_4C_x Molybdenum Carbide Nanoparticles and Their Anchoring Sites on ZSM-5 Zeolites. *J. Phys. Chem. C* **2014**, *118*, 4670−4679.

(13) Prats, H.; Piñero, J. J.; Viñes, F.; Bromley, S. T.; Sayós, R.; Illas, F. Assessing the Usefulness of Transition Metal Carbides for Hydrogenation Reactions. *Chem. Commun.* **2019**, *55*, 12797−12800.

(14) Jiménez-Orozco, C.; Flórez, E.; Viñes, F.; Rodriguez, J. A.; Illas, F. Critical Hydrogen Coverage Effect on the Hydrogenation of Ethylene Catalyzed by δ-MoC(001): An *Ab Initio* Thermodynamic and Kinetic Study. *ACS Catal.* **2020**, *10*, 6213−6222.

(15) Figueras, M.; Gutiérrez, R. A.; Prats, H.; Viñes, F.; Ramírez, P. J.; Illas, F.; Rodriguez, J. A. Boosting the Activity of Transition Metal Carbides Towards Methane Activation by Nanostructuring. *Phys. Chem. Chem. Phys.* **2020**, *22*, 7110−7118.

(16) Graciani, J.; Mudiyanselage, K.; Xu, F.; Baber, A. E.; Evans, J.; Senanayake, S. D.; Stacchiola, D. J.; Liu, P.; Hrbek, J.; Sanz, J. F.; Rodriguez, J. A. Highly Active Copper-ceria and Copper-ceria-titania Catalysts for Methanol Synthesis from CO_2. *Science* **2014**, *345*, 546−550.

(17) Horn, J. M.; Song, Z.; Potapenko, D. V.; Hrbek, J.; White, M. G. Characterization of Molybdenum Carbide Nanoparticles Formed on Au(111) Using Reactive-Layer Assisted Deposition. *J. Phys. Chem. B* **2005**, *109*, 44−47.

(18) Potapenko, D. V.; Horn, J. M.; White, M. G. The Reactions of Cyclohexene on Au(111)-supported Molybdenum Carbide Nanoparticles. *J. Catal.* **2005**, *236*, 346−355.

(19) Baddour, F. G.; Roberts, E. J.; To, A. T.; Wang, L.; Habas, S. E.; Ruddy, D. A.; Bedford, N. M.; Wright, J.; Nash, C. P.; Schaidle, J. A.; Brutchey, R. L.; Malmstadt, N. An Exceptionally Mild and Scalable Solution-Phase Synthesis of Molybdenum Carbide Nanoparticles for Thermocatalytic CO_2 Hydrogenation. *J. Am. Chem. Soc.* **2020**, *142*, 1010−1019.

(20) Posada-Pérez, S.; Ramírez, P. J.; Evans, J.; Viñes, F.; Liu, P.; Illas, F.; Rodriguez, J. A. Highly Active Au/δ-MoC and Cu/δ-MoC Catalysts for the Conversion of CO_2: The Metal/C Ratio as a Key Factor Defining Activity, Selectivity, and Stability. *J. Am. Chem. Soc.* **2016**, *138*, 8269−8278.

(21) Piñero, J. J.; Ramírez, P. A.; Bromley, S. T.; Illas, F.; Viñes, F.; Rodriguez, J. A. Diversity of Adsorbed Hydrogen on the TiC(001) Surface at High Coverages. *J. Phys. Chem. C* **2018**, *122*, 28013−28020.

(22) Christmann, K.; Ertl, G.; Pignet, T. Adsorption of Hydrogen on a Pt(111) Surface. *Surf. Sci.* **1976**, *54*, 365−392.

(23) Perdew, J. P.; Burke, K.; Ernzerhof, M. Generalized Gradient Approximation Made Simple. *Phys. Rev. Lett.* **1996**, *77*, 3865−3868.

(24) Grimme, S.; Antony, J.; Ehrlich, S.; Krieg, S. A. A Consistent and Accurate *Ab Initio* Parametrization of Density Functional Dispersion Correction (DFT-D) for the 94 Elements H-Pu. *J. Chem. Phys.* **2010**, *132*, 154104.